Electronic Supplementary Information (ESI) for

Stereoselective photoreaction in P-stereogenic dithiazolylbenzo[*b*]phosphole chalcogenides

Shunsuke Iijima,[a] Takuya Nakashima[a] and Tsuyoshi Kawai[a,b*]

[a] *Graduate School of Materials Science, Nara Institute of Science and Technology, NAIST, 8916-5 Takayama, Ikoma, Nara, 630-0192, Japan.*
E mail: tkawai@ms.naist.jp
[b] *NAIST-CEMES International Collaborative Laboratory for Supraphotoactive System, Centre d'Élaboration de Matériaux et d'Etudes Structurales, CEMES,*
29, rue Jeanne Marvig, BP 94347, Toulouse 31055, France.

1. NMR characterizations

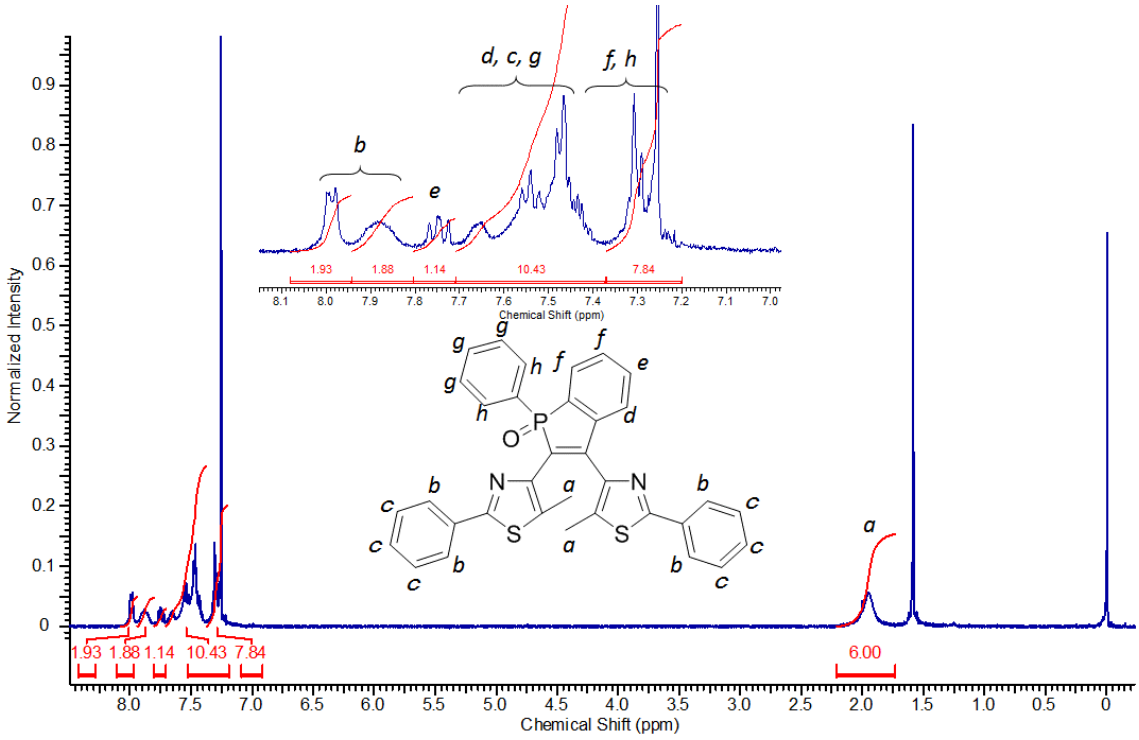

Fig. S1 ^{1}H NMR spectrum of ***rac*-1a** in $CDCl_3$.

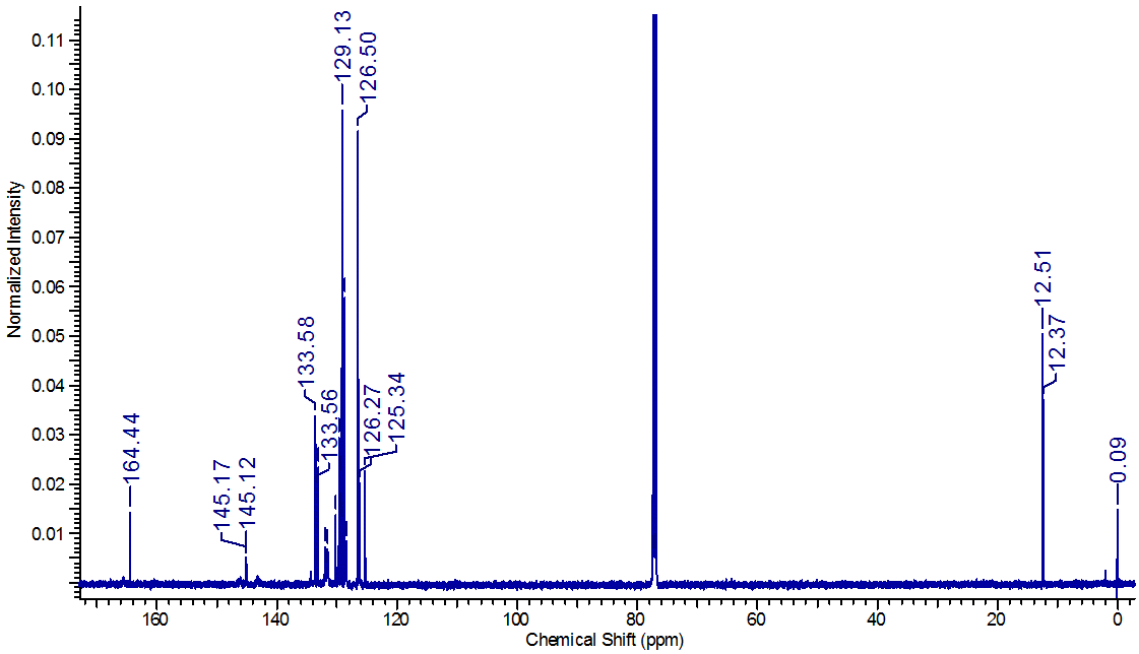

Fig. S2 ^{13}C NMR spectrum of ***rac*-1a** in $CDCl_3$.

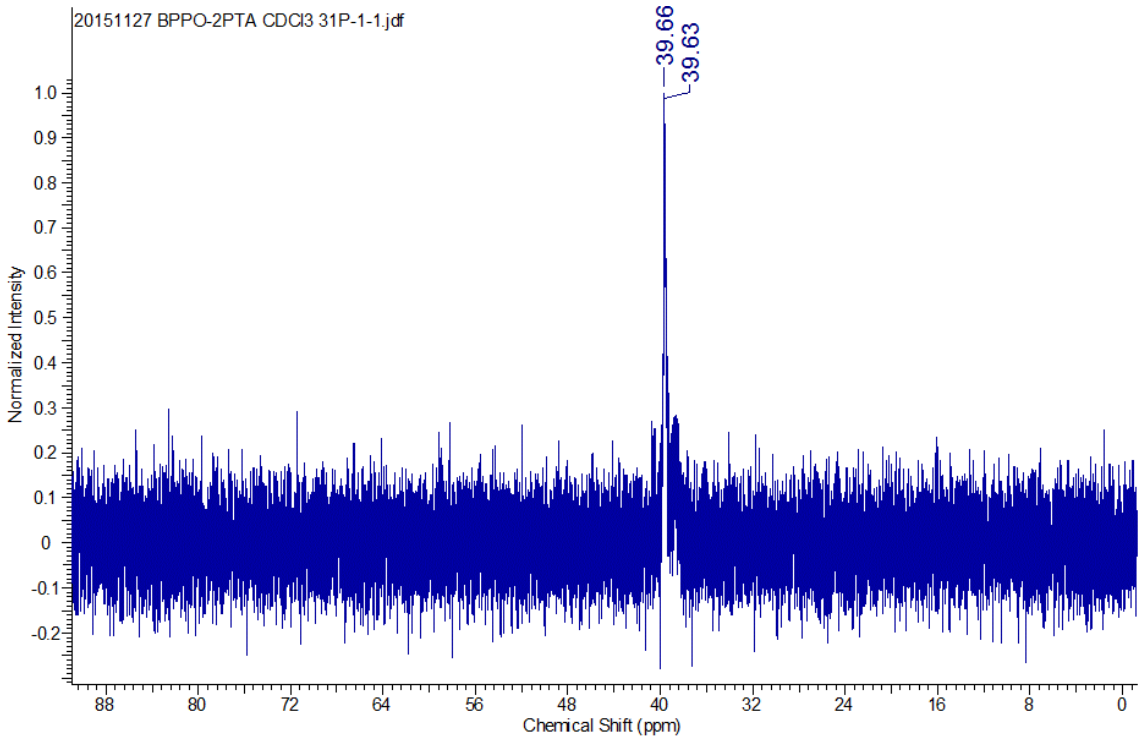

Fig. S3 ^{31}P NMR spectrum of ***rac*-1a** in $CDCl_3$.

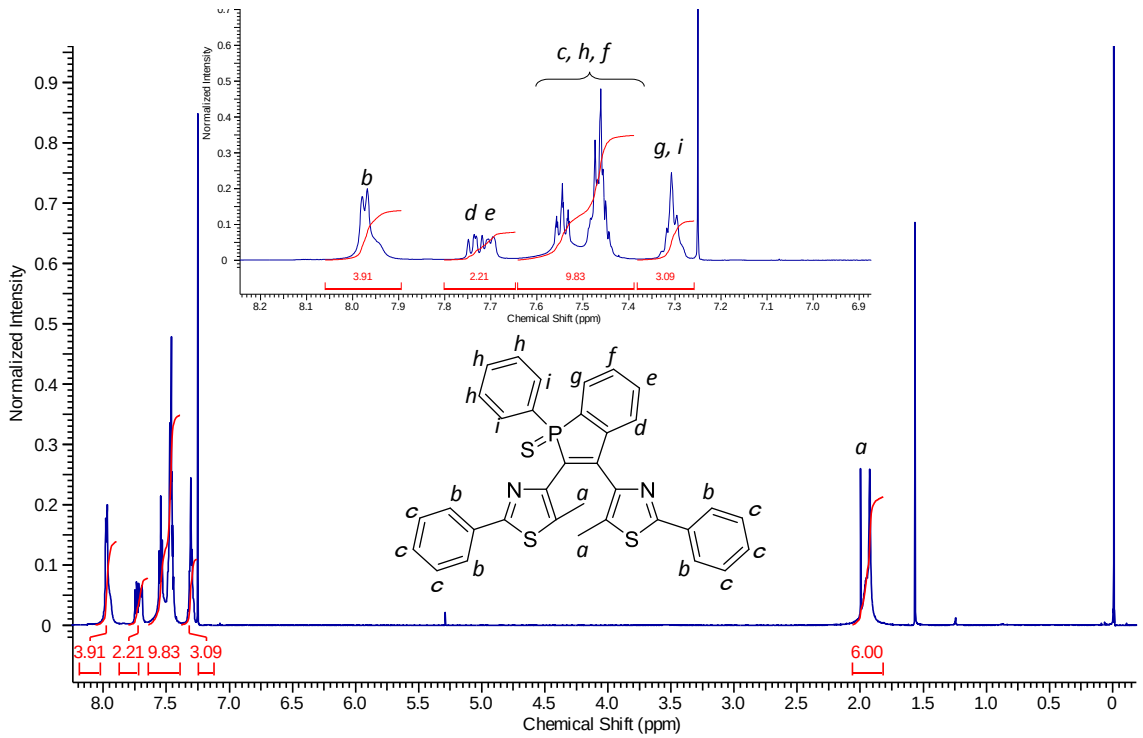

Fig. S4 ^{1}H NMR spectrum of ***rac*-2a** in $CDCl_3$.

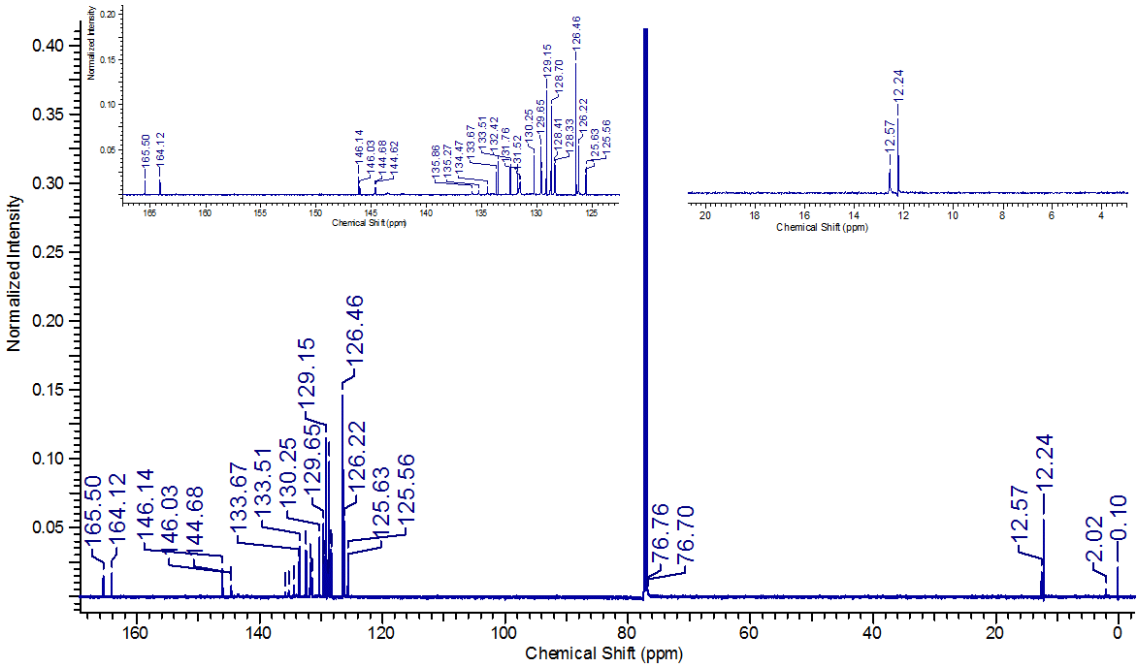

Fig. S5 ^{13}C NMR spectrum of ***rac*-2a** in $CDCl_3$.

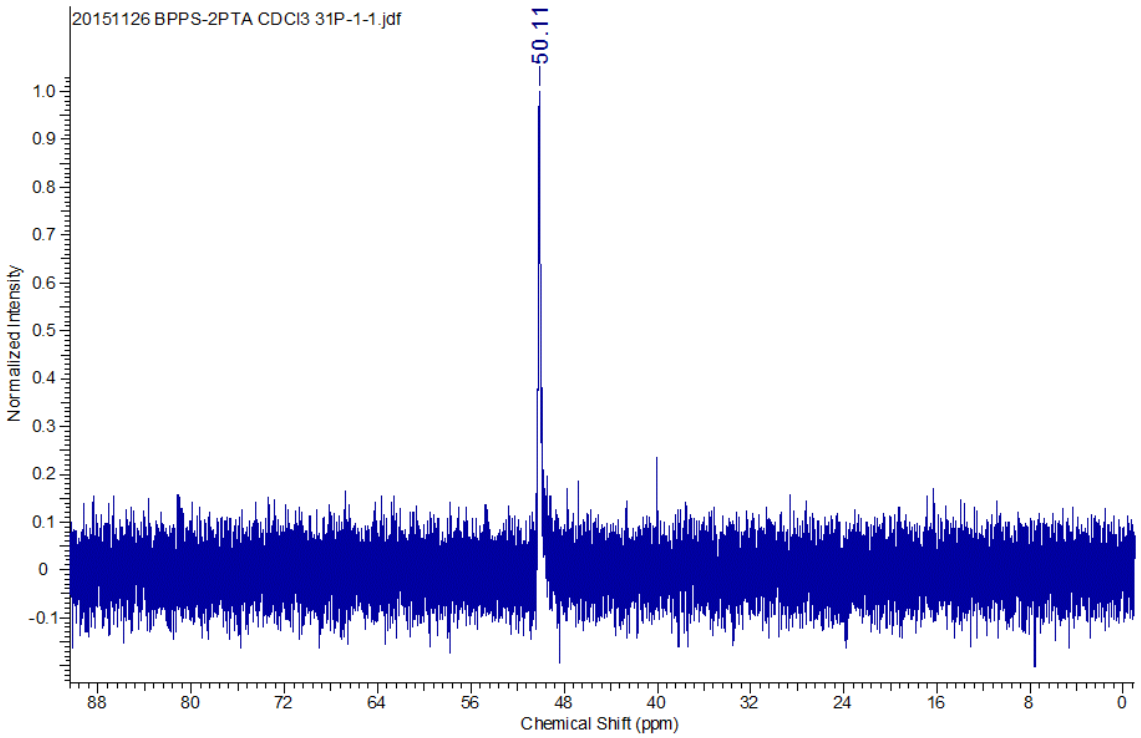

Fig. S6 ^{31}P NMR spectrum of ***rac*-1a** in $CDCl_3$.

2. Photoreaction monitored with UV-vis spectra and ^{1}H NMR

2.1. UV-Vis absorption spectral change

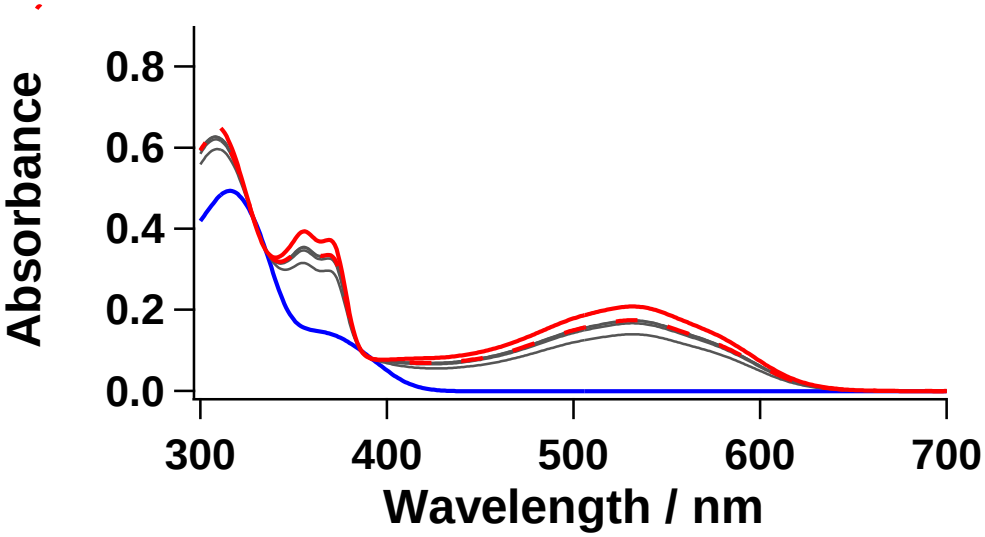

Fig. S7 Changes in the UV-vis absorption spectra of open form (***rac*-1a**, blue solid line) to PSS (red dashed line), and closed form (**1b**, red solid line) in toluene (1.9×10^{-5} M).

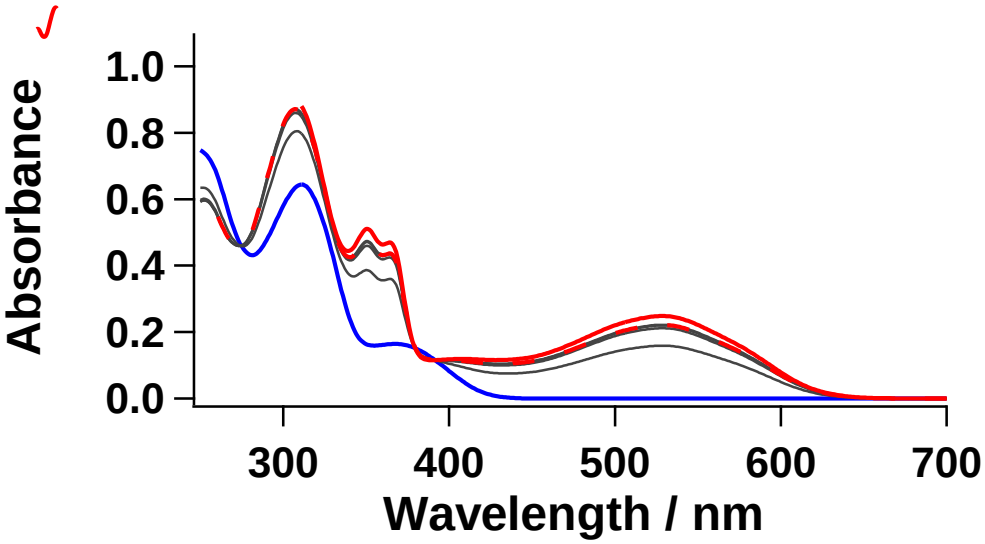

Fig. S8 Changes in the UV-Vis absorption spectra of open form (***rac*-1a**, blue solid line) to PSS (red dashed line), and closed form (**1b**, red solid line) in methanol (2.3×10^{-5} M).

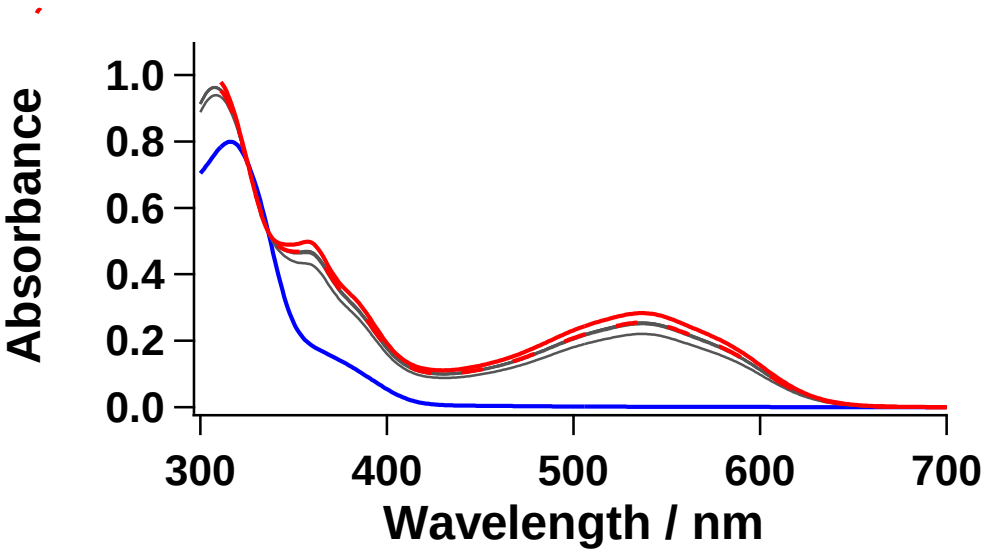

Fig. S9 Changes in the UV-Vis absorption spectra of open form (***rac*-2a**, blue solid line) to PSS (red dashed line), and closed form (**2b**, red solid line) in toluene (2.9×10^{-5} M).

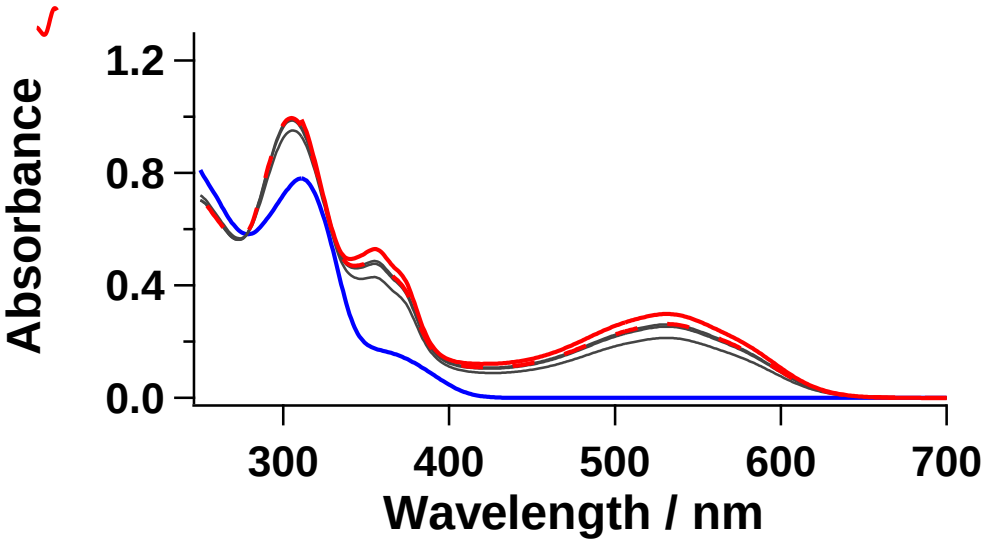

Fig. S10 Changes in the UV-Vis absorption spectra of open form (***rac*-2a**, blue solid line) to PSS (red dashed line), and closed form (**2b**, red solid line) in methanol (2.8×10^{-5} M).

2.2. ^{1}H NMR spectral change

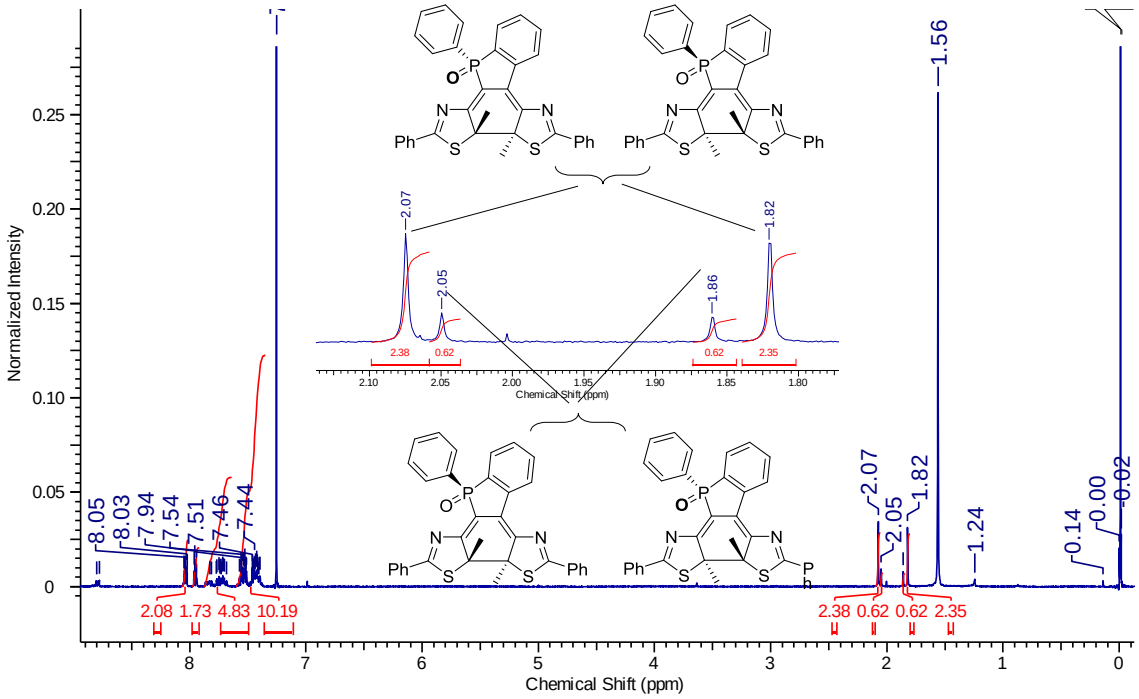

Fig. S11 ^{1}H NMR spectrum of photoproducts **1b** prepared by UV irradiation to the toluene solution followed by the separated with RP-HPLC (measured in $CDCl_3$).

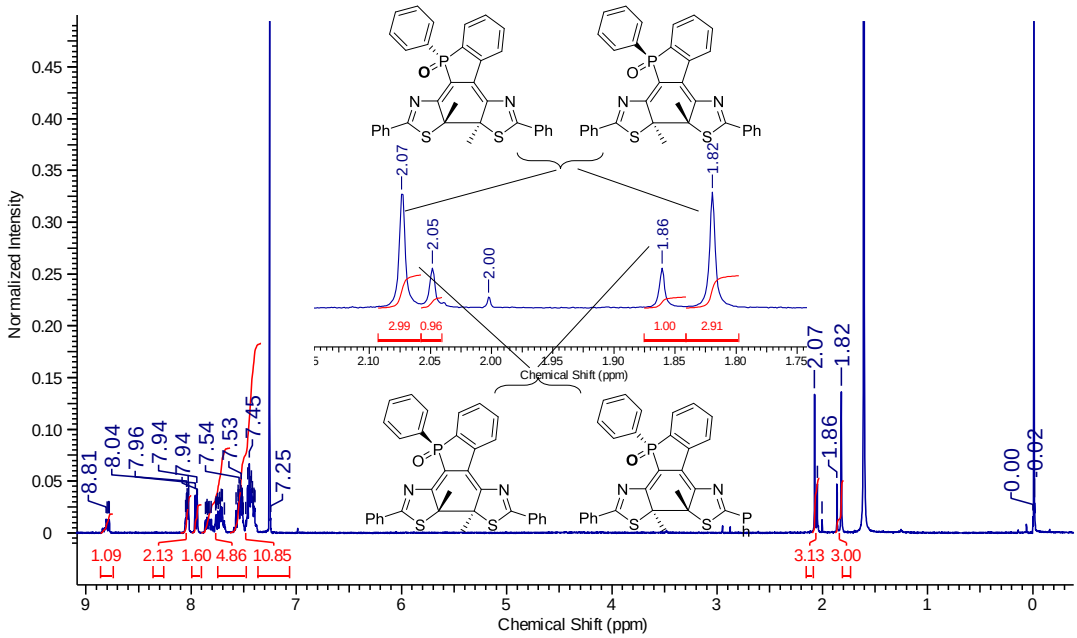

Fig. S12 ^{1}H NMR spectrum of photoproducts **1b** prepared by UV irradiation to the methanol solution followed by the separated with RP-HPLC (measured in $CDCl_3$).

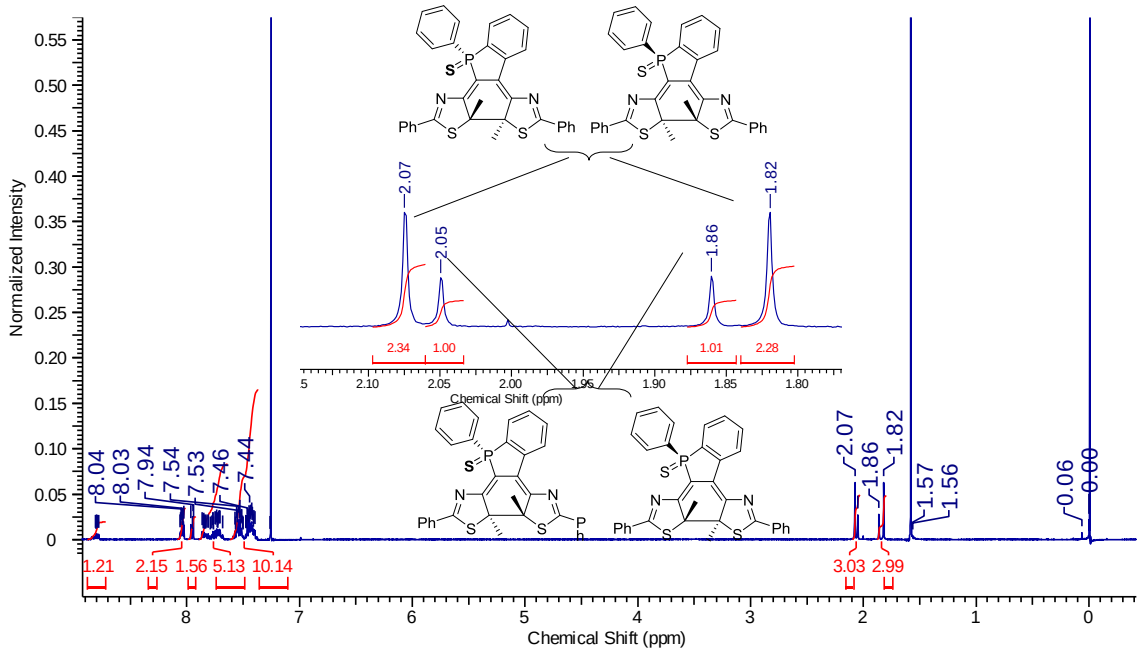

Fig. S13 ^{1}H NMR spectrum of photoproducts **2b** prepared by UV irradiation to the toluene solution followed by the separated with RP-HPLC (measured in $CDCl_3$).

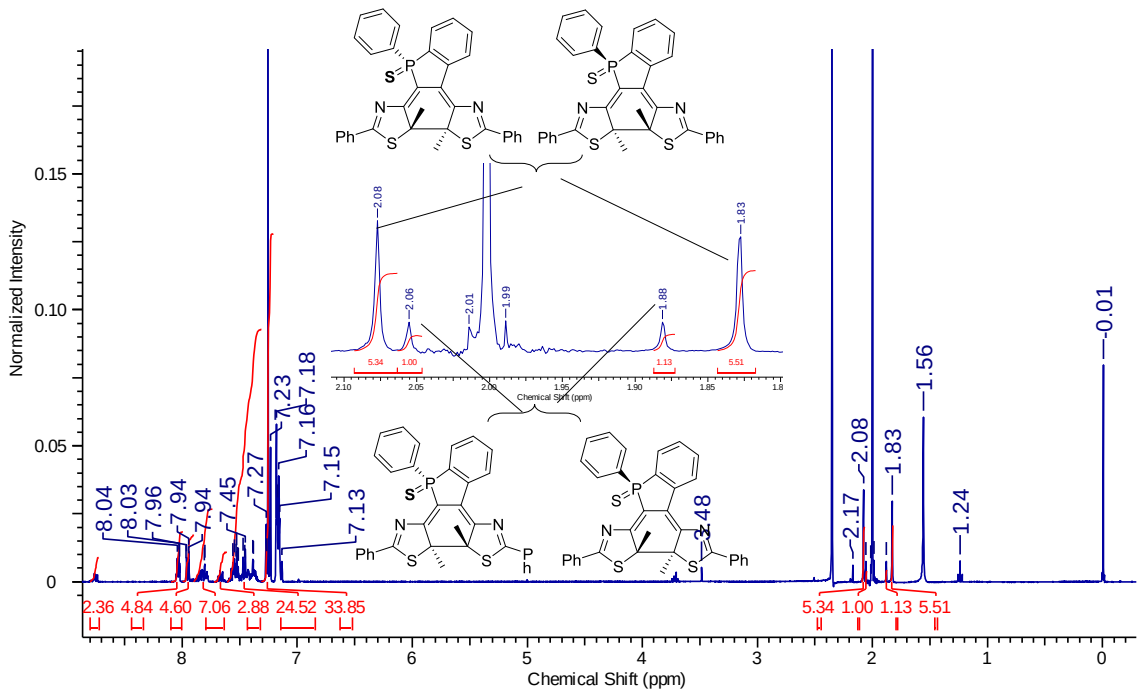

Fig. S14 ^{1}H NMR spectrum of photoproducts **2b** prepared by UV irradiation to the methanol solution followed by the separated with RP-HPLC (measured in $CDCl_3$).

3. Chiral separation

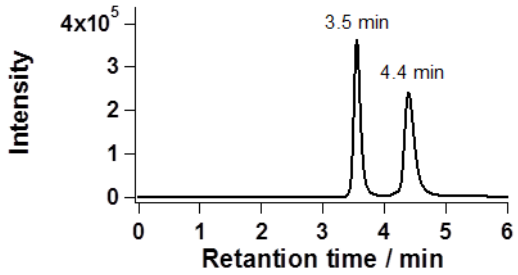

Fig. S15 Chiral HPLC chromatogram of ***rac*-1a** in ethanol. (Flow rate: 6 mL / min., Detection wavelength: 254 nm)

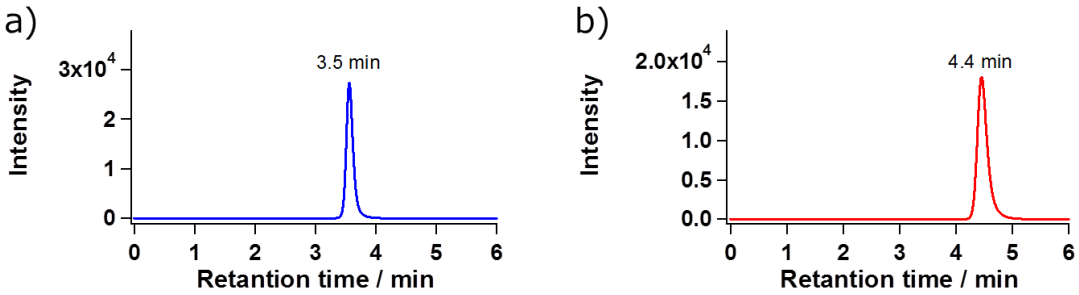

Fig. S16 Chiral HPLC chromatogram of a) primary fraction and b) second fraction separated of ***rac*-1a** in ethanol, after optical resolution. (Flow rate: 6 mL / min., Detection wavelength: 254 nm)

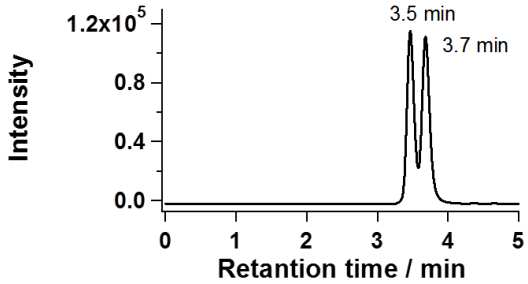

Fig. S17 Chiral HPLC chromatogram of ***rac*-2a** in ethanol. (Flow rate: 6 mL / min., Detection wavelength: 254 nm)

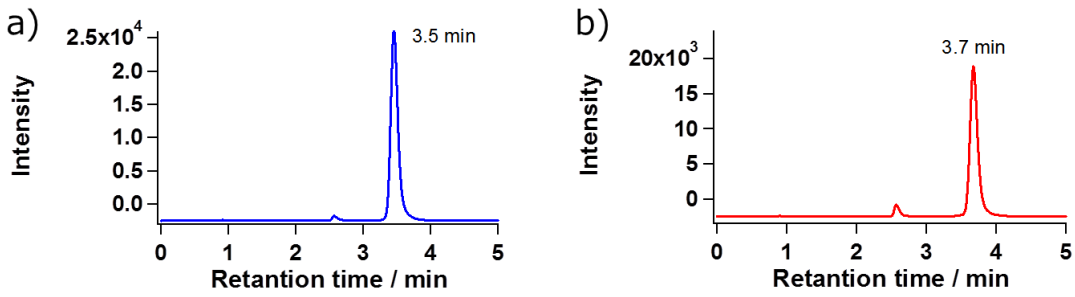

Fig. S18 Chiral HPLC chromatogram of a) primary fraction and b) second fraction separated of ***rac*-2a** in ethanol, after optical resolution. (Flow rate: 6 mL / min., Detection wavelength: 254 nm)

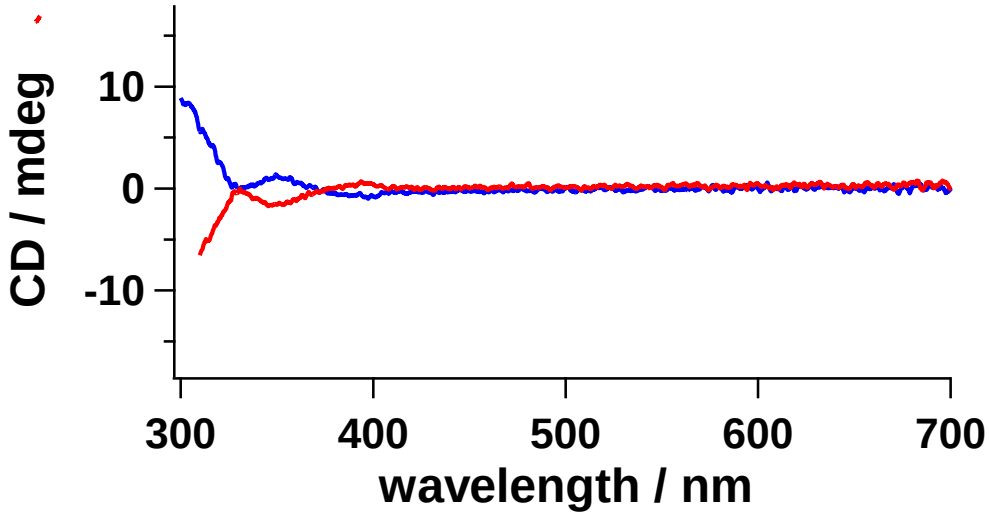

Fig. S19 CD spectra for ***rac*-1a** of open form in toluene (blue: first fraction, red: second fraction).

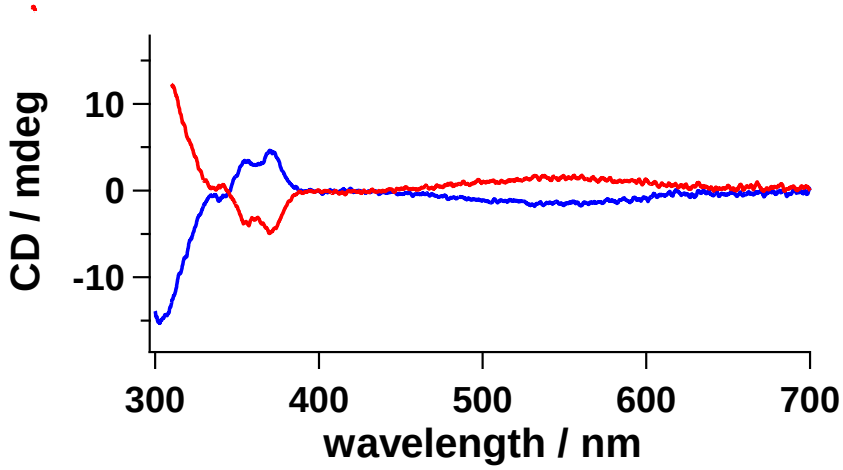

Fig. S20 CD spectra at PSS states achieved by UV irradiation to the solution in **Fig. S15** in toluene.

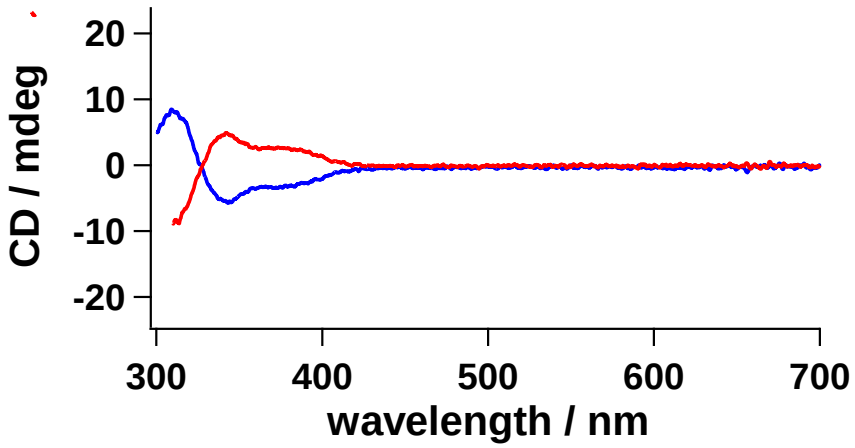

Fig. S21 CD spectra for ***rac*-2a** of open form in toluene (blue: first fraction, red: second fraction).

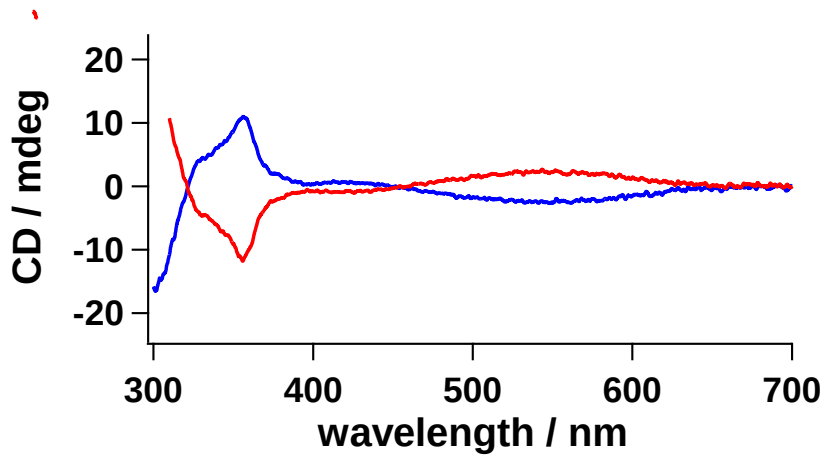

Fig. S22 CD spectra at PSS states achieved by UV irradiation to the solution in **Fig. S17** in toluene.

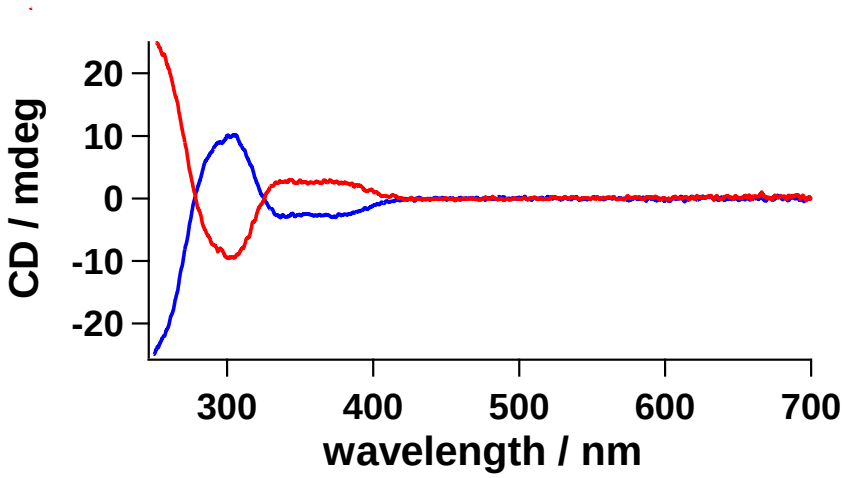

Fig. S23 CD spectra for ***rac*-2a** of open form in methanol (blue: first fraction, red: second fraction).

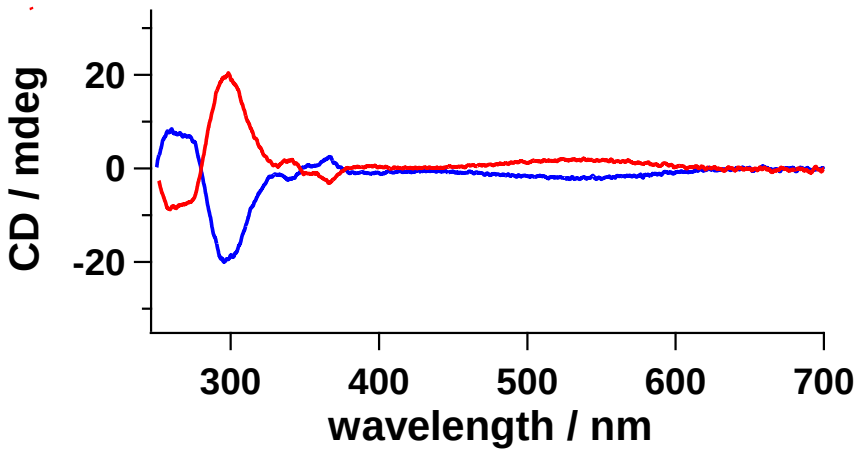

Fig. S24 CD spectra at PSS states achieved by UV irradiation to the solution in **Fig. S19** in methanol.

4. Study in crystalline state

4.1 Photochromism in crystal

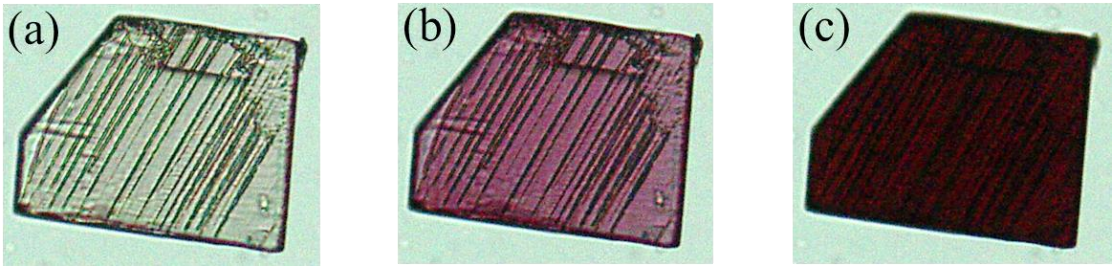

Fig. S25 Photochromism of ***rac*-1a** in crystal; (a) before and after (b,c) UV irradiation.

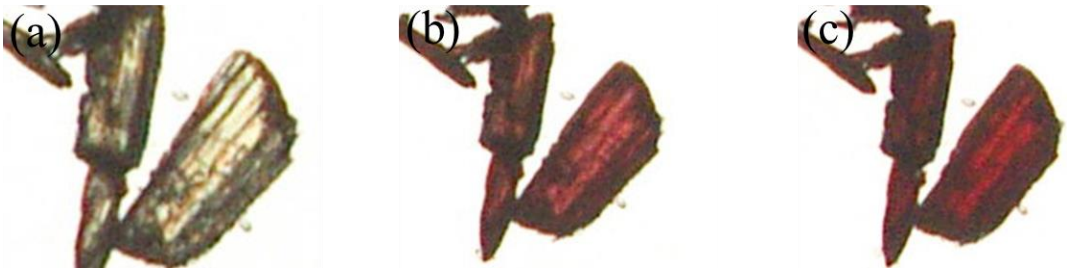

Fig. S26 Photochromism of ***rac*-2a** in crystal; (a) before and after (b,c) UV irradiation.

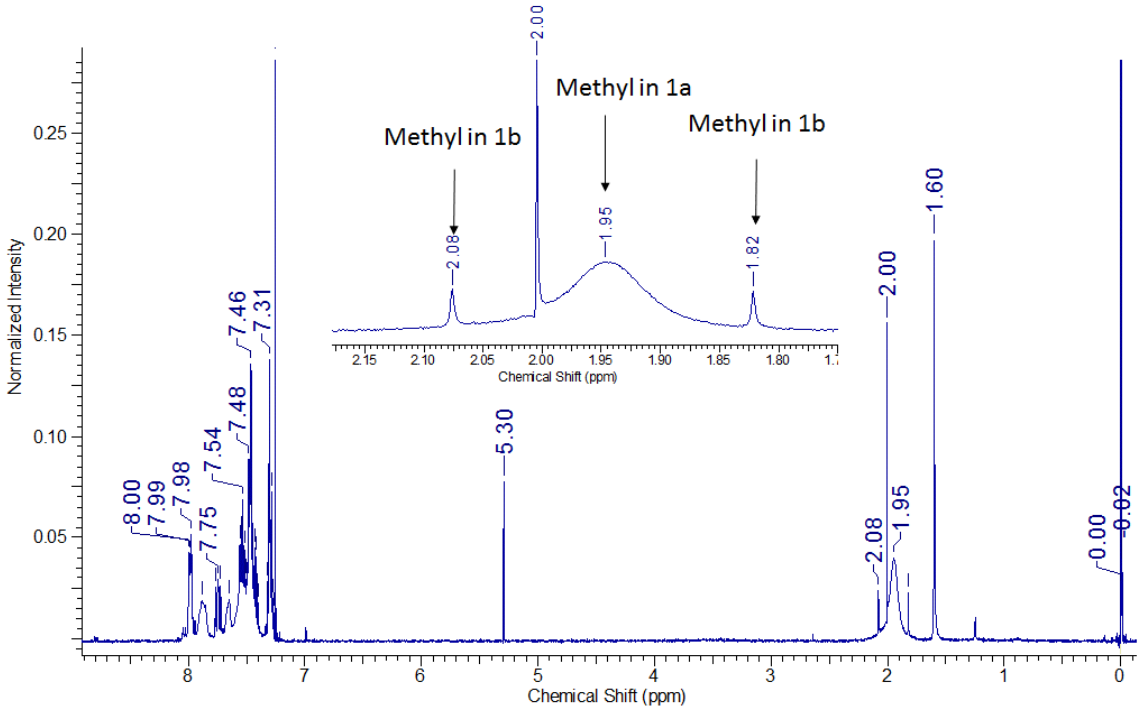

Fig. S27 ^{1}H NMR spectrum of photoproducts prepared by UV irradiation to single crystals **1a** and dissolved in $CDCl_3$.

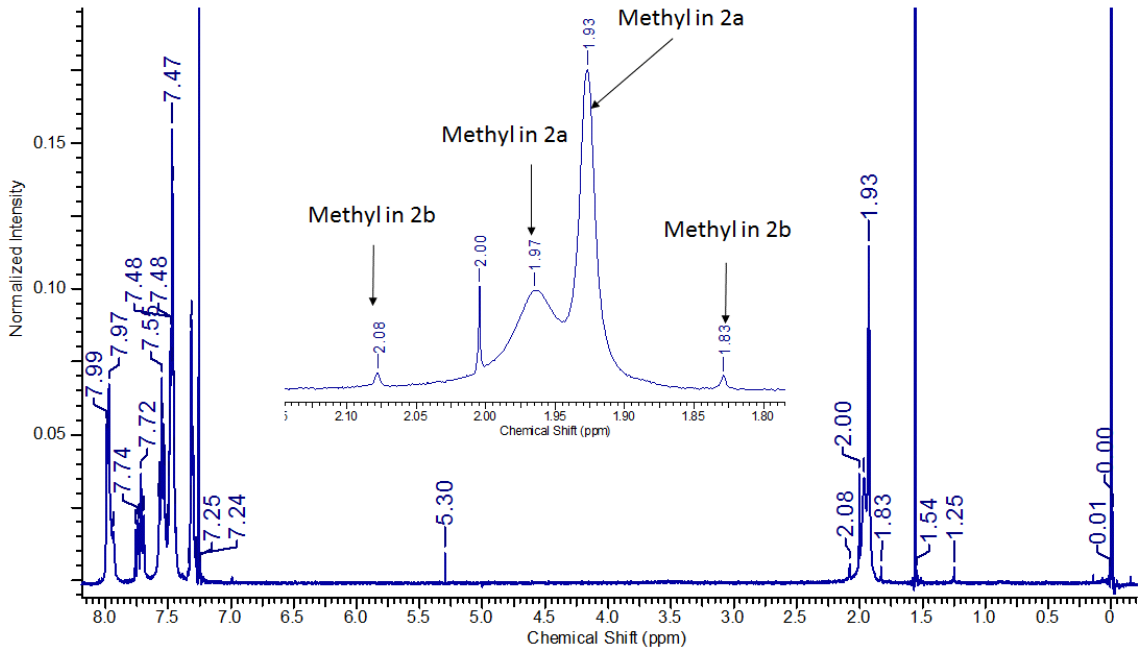

Fig. S28 ^{1}H NMR spectrum of photoproducts prepared by UV irradiation to single crystals **1b** and dissolved in $CDCl_3$.

4.2 X-ray crystallographic data

Table S1. Crystallographic data for ***rac*-1a** and ***rac*-2a**

Molecule	***rac*-1a**	***rac*-2a**
Formula	$C_{34}H_{25}N_2OPS_2$	$C_{36}H_{28}N_3PS_3$
Mol weight (g mol^{-1})	572.68	629.79
Crystal dimension (mm)	0.100 × 0.070 × 0.020	0.140 × 0.100 × 0.050
Crystal system	Monoclinic	Triclinic
Space group	$P2_{1/c}$ (#14)	$P\bar{1}$ (#2)
a (Å)	11.4597(2)	10.0101(2)
b (Å)	29.0720(5)	11.0471(2)
c (Å)	16.6209(3)	14.5019(3)
α (°)		86.1262(7)
β (°)	93.7884(7)	83.4645(7)
γ (°)		81.5450(7)
V (Å^3)	5525.24(17)	1573.81(5)
Z value	8	2
D_{calcd} (g mol^{-1})	1.377	1.329
F (0 0 0)	2384.00	656.00
μ (Mo Kα) (cm^{-1})	2.825	3.171
Temperature (K)	123	123
No. of measured reflections	95332	27280
No. of unique reflections	12666	7207
Goodness of fit	1.05	1.09
Final R indices		
R_1	0.0395	0.0374
wR_2 [$I > 2\sigma(I)$]	0.0997	0.1026
CCDC No.	CCDC-1445542	CCDC-1445543

5. Computational data

Optimization of molecular conformations of **1a** and **2a** were carried out by DFT calculation with ωB97XD/6-31G(d,p) level.

5.1. Optimization of molecular conformation

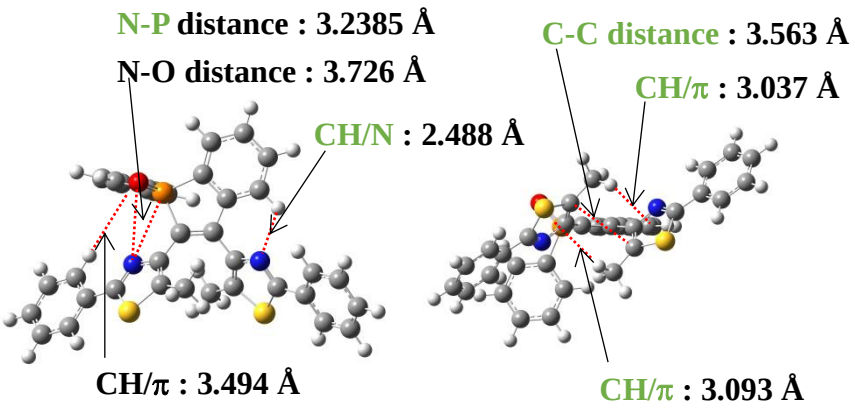

Fig. S29 Optimized structure of ***S*P-*P*-1a**.

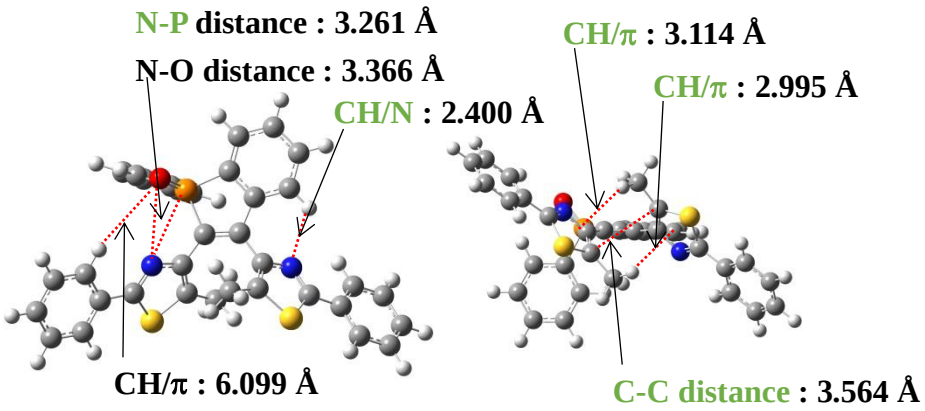

Fig. S30 Optimized structure of ***S*P-*M*-1a**.

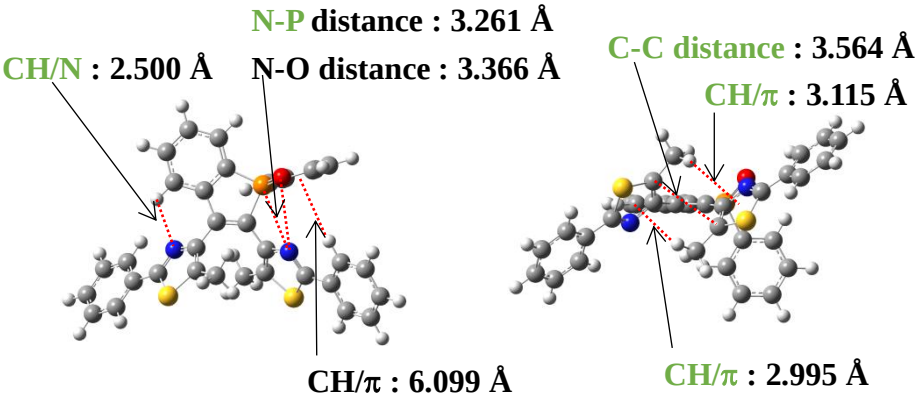

Fig. S31 Optimized structure of ***R*$_P$-*P*-1a**.

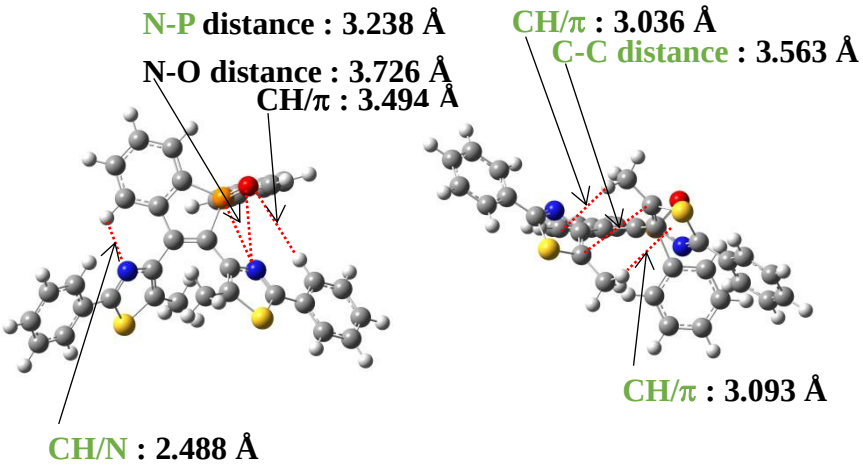

Fig. S32 Result of optimization of ***R*$_P$-*M*-1a**.

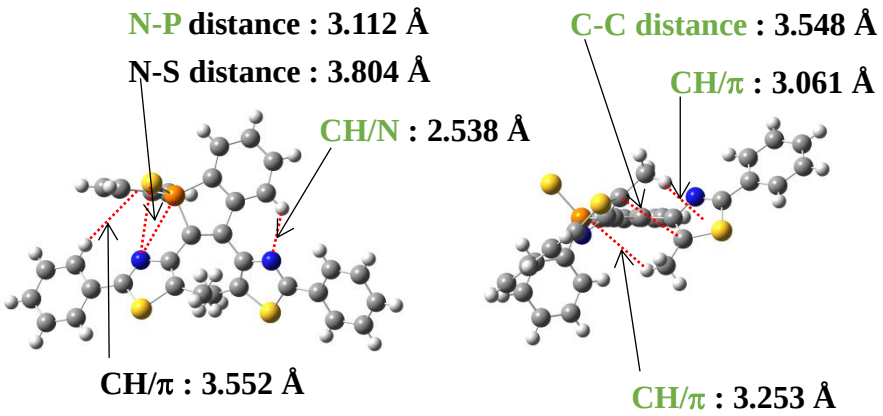

Fig. S33 Optimized structure of ***S*$_P$-*P*-2a**.

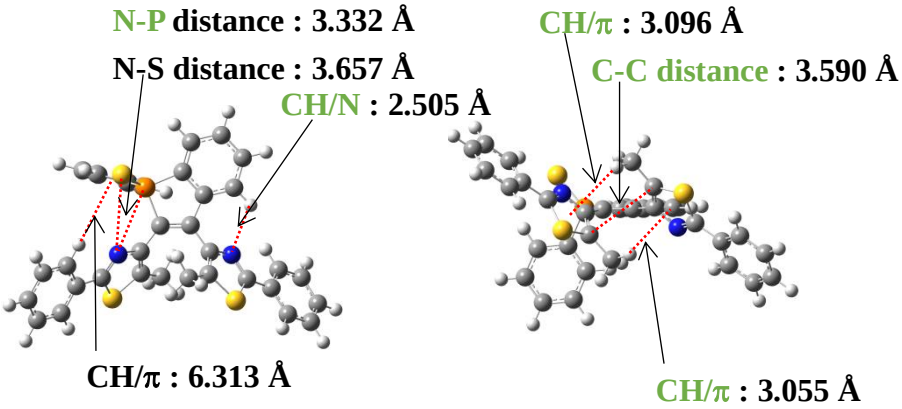

Fig. S34 Optimized structure of ***S*$_P$-*M*-2a**.

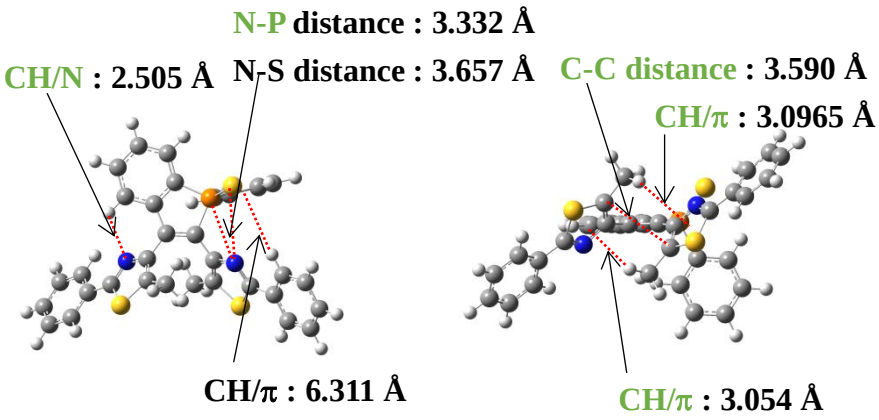

Fig. S35 Optimized structure of ***R*$_P$-*P*-2a**.

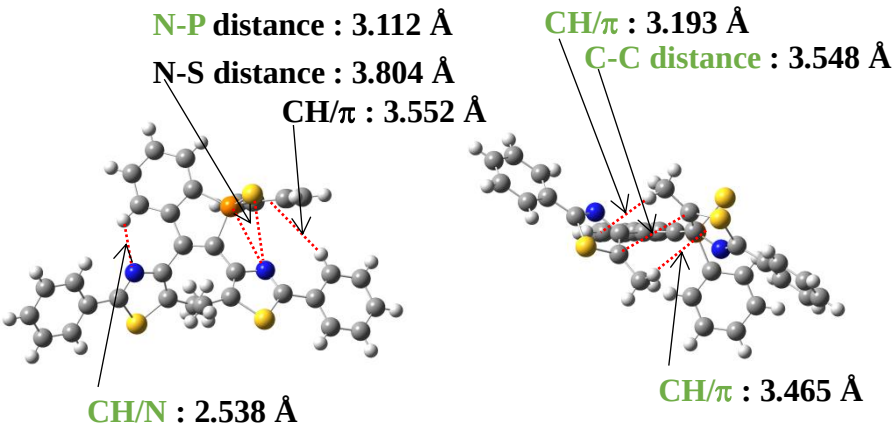

Fig. S36 Optimized structure of ***R*$_P$-*M*-2a**.

5.2. Energy difference between *P*- and *M*-conformers estimated by DFT

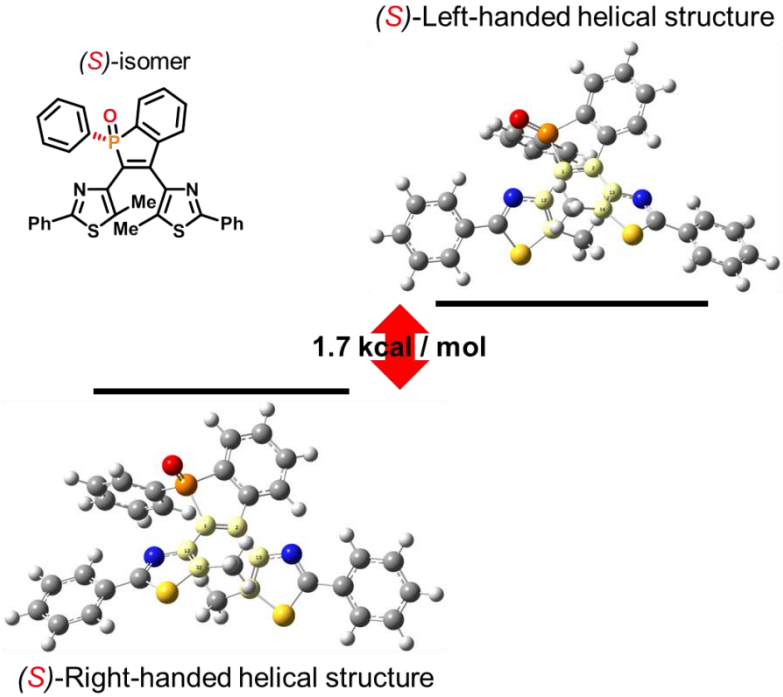

Fig. S37 Diagram of energy difference between ***S*P-*P*-1a** and ***S*P-*M*-1a** optimized by ωB97XD/6-31G(d,p) level of DFT calculation.

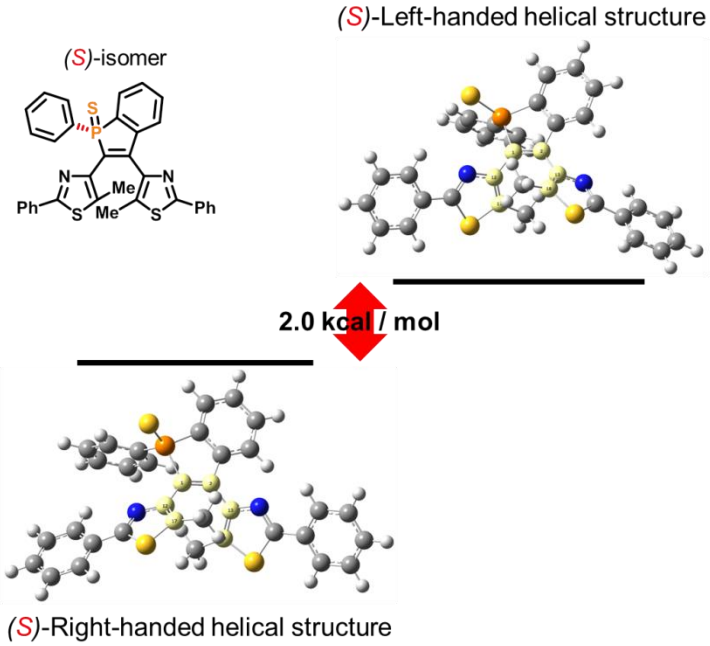

Fig. S38 Diagram of energy difference between ***S*P-*P*-2a** and ***S*P-*M*-2a** optimized by ωB97XD/6-31G(d,p) level of DFT calculation.

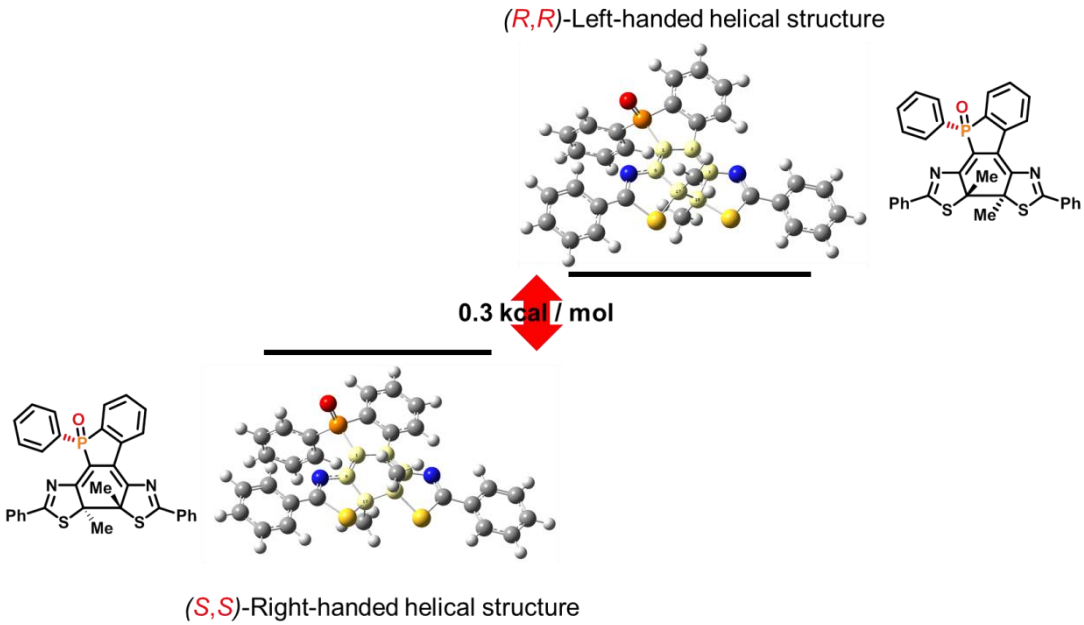

Fig. S39 Diagram of energy difference between diastereomers of ***S*P-*(R,R)*-1b** and ***S*P-(*S,S*)-1b** calculated by CAM-B3LYP/6-31G(d,p) level of DFT calculation.

6. Other NMR data

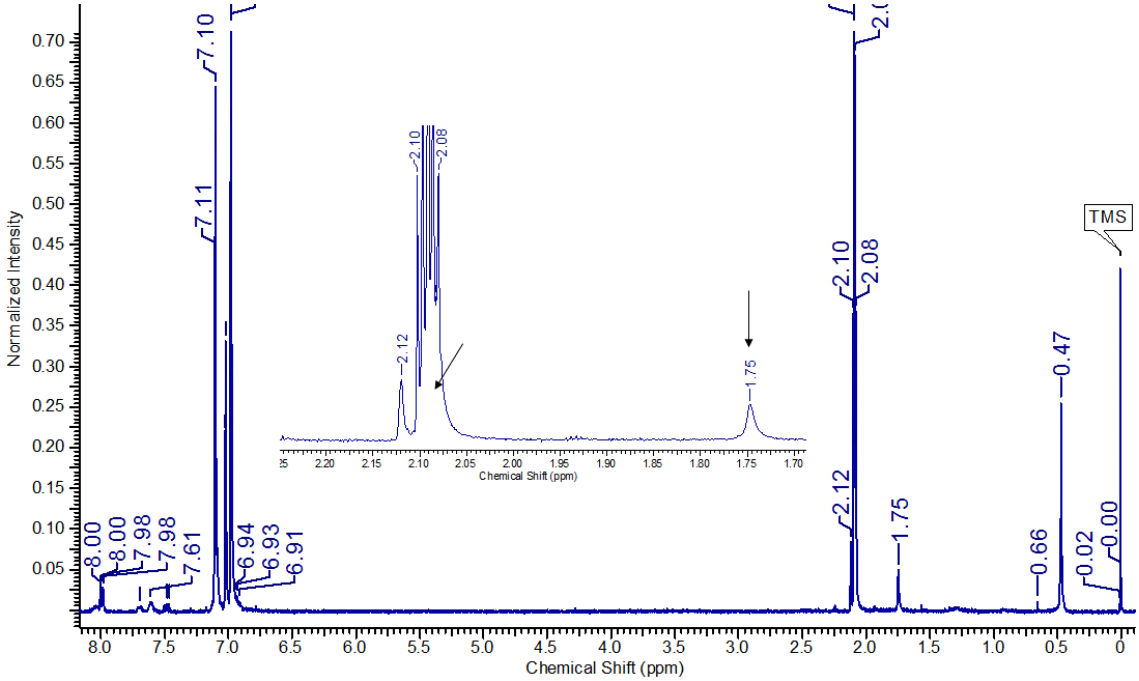

Fig. S40 ^{1}H NMR spectrum of ***rac*-1a** in toluene-d_8.

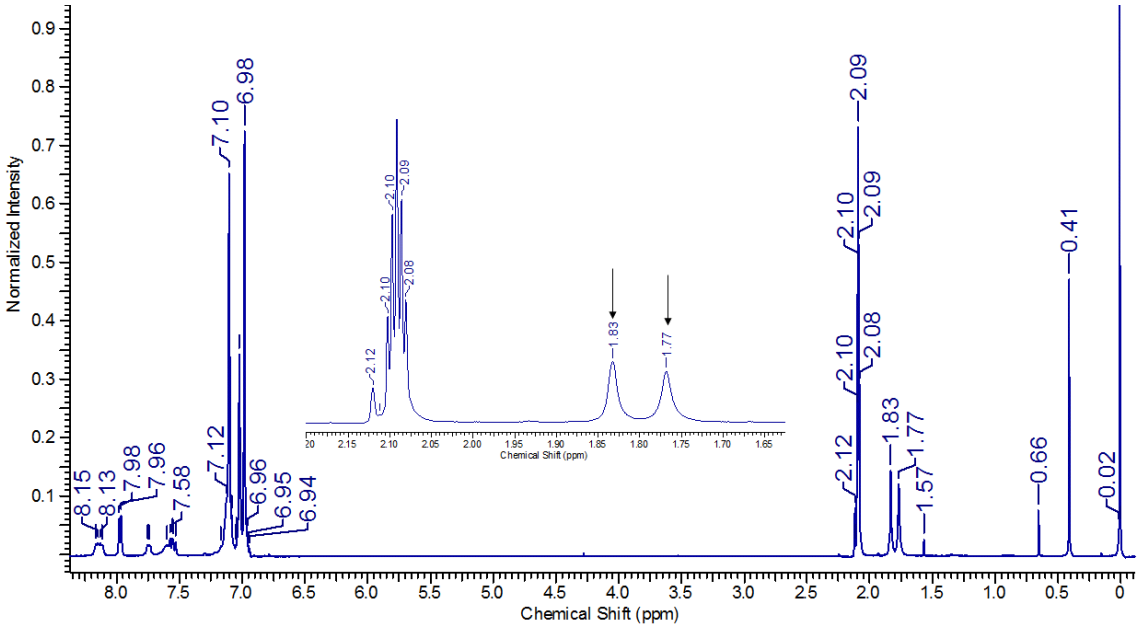

Fig. S41 ^{1}H NMR spectrum of ***rac*-2a** in toluene-d_8.

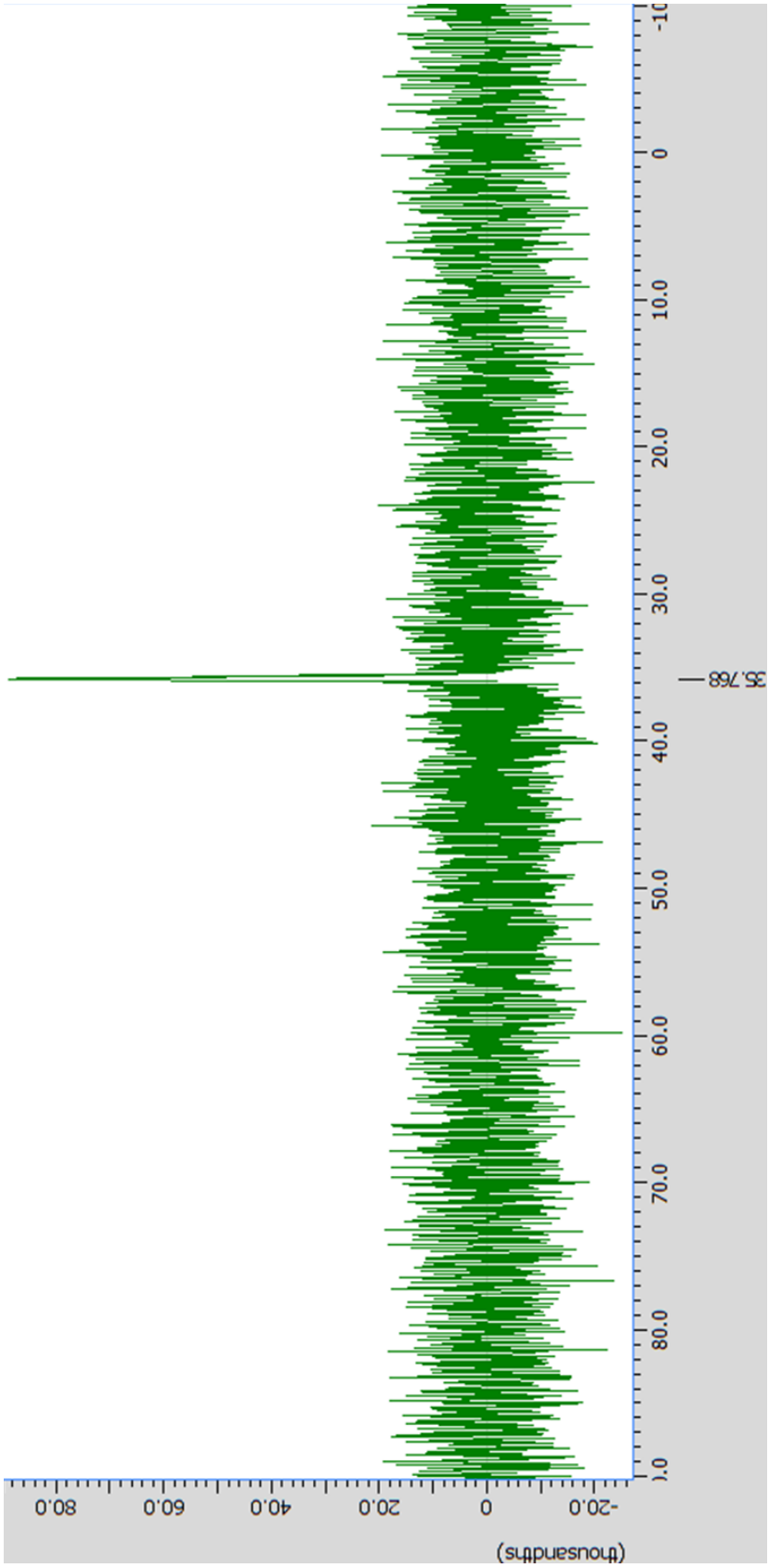

Fig. S42 ^{31}P NMR spectrum of ***rac*-1a** in toluene-d_8.

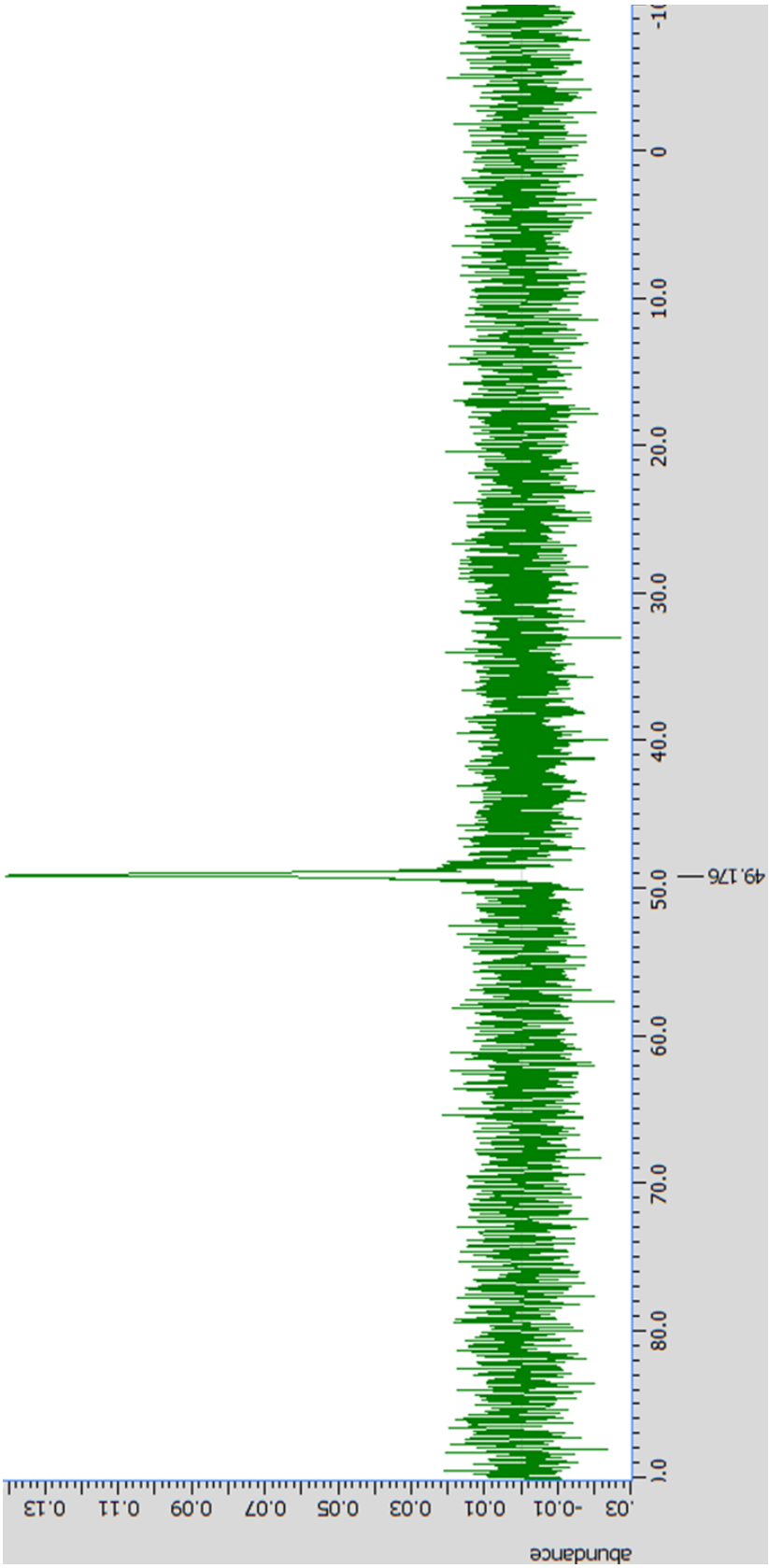

Fig. S43 ^{31}P NMR spectrum of ***rac*-2a** in toluene-d_8.